Primary Lung Cancer SPECT Imaging with Pentavalent Technetium-99m-DMSA

Tsuneo Hirano, Hidenori Otake, Ichiro Yoshida and Keigo Endo

Departments of Nuclear Medicine and Surgery, Gunma University, School of Medicine, Gunma Japan

To assess the clinical role of ^{99m}Tc(V)-DMSA in primary lung cancers, SPECT imaging was performed on 31 patients with suspected lung cancer. **Methods:** Planar and SPECT images were obtained at 3 to 4 hr after intravenous injection of approximately 555 MBq ^{99m}Tc(V)-DMSA. Two uptake ratios (the maximum counts/pixel in the lesion to the average counts in normal tissue) were calculated. **Results:** Various types of primary lung cancers (adenocarcinoma, squamous-cell carcinoma, small-cell carcinoma, large-cell carcinoma and bronchial carcinoid tumor) were imaged by ^{99m}Tc(V)-DMSA SPECT. Approximately 90% of the lung carcinomas showed increased uptake and were clearly demonstrated by SPECT images. Four cases incidentally revealed osseous metastatic lesion. Three benign lesions did not show increased uptake. Three cases were false-negative and there were no false-positive cases for the primary lesions. **Conclusion:** Technetium-99m(V)-DMSA SPECT images demonstrated approximately 90% of the primary lung cancers. Uptake ratios were higher in squamous-cell carcinomas than adenocarcinomas. Evaluation of mediastinal tumor extension and nodal metastatic lesion was very difficult by high blood-pool activity in the major cardiovascular structures due to slow blood-pool clearance. However, ^{99m}Tc(V)-DMSA SPECT imaging was very useful for detecting primary lung cancers and metastatic lesions to the osseous structures.

Key Words: pentavalent technetium-99m-DMSA; primary lung cancer; tumor imaging; osseous metastatic disease

J Nucl Med 1995; 36:202–207

Pentavalent ^{99m}Tc-dimercaptosuccinic acid (^{99m}Tc(V)-DMSA) is a tumor imaging agent (*1–3*) that accumulates in the medullary carcinoma of the thyroid (*4–6*), soft-tissue tumors (*7–8*) and bone metastasis (*9*). There also have been a number of reports on evaluating biodistribution and detecting squamous-cell carcinoma (SCC) both in humans (*10–11*) and in animal tumor models (*12*). Recently, we established a simple method for preparing ^{99m}Tc(V)-DMSA from a commercially available DMSA kit and evaluated primary lung tumors using ^{99m}Tc(V)-DMSA and SPECT.

Received Mar. 16, 1994; revision accepted Nov. 1, 1994.

For correspondence or reprints contact: Tsuneo Hirano, MD, Department of Nuclear Medicine, Gunma University, School of Medicine, 3-39-15 Showa-machi, Maebashi, Gunma 00371, Japan.

MATERIALS AND METHODS

Patients with a lung tumor were selected for imaging. Chest-radiographs, CT and cytological examinations were performed. Patients with positive malignant cytology and malignant feature on imaging were treated by operation and/or irradiation. Final pathological diagnoses were obtained from the surgical or biopsy (TBLB) specimens. Pre- or postoperative staging was obtained according to the TNM clinical classification of The Japan Lung Cancer Society and stage grouping. Patients with negative histological finding and benign feature on imaging by repeat examinations were regularly followed up.

The Techne® DMSA kit (Daiichi Radioisotope, Tokyo, Japan) contains 1.4 mg DMSA and 0.5 mg $SnCl_2 \cdot 2H_2O$. A DMSA kit with an additional 200 μl of 7% of sodium bicarbonate solution ($NaHCO_3$) was reconstituted with 2 ml of [^{99m}Tc]pertechnetate solution (~740 MBq) (*13*). Planar and SPECT images were obtained 3 to 4 hr after intravenous administration of approximately 555 MBq of ^{99m}Tc(V)-DMSA with a rotating single-headed gamma camera equipped with a high-resolution and a low-energy, all-purpose collimator for planar and SPECT imaging, respectively. The camera was connected to a nuclear medicine computer (Scintipac-700, Schimadzu Corporation, Kyoto, Japan). Planar images (128 × 128 matrix) were acquired for 5 min each. SPECT images (64 × 64 matrix) were acquired using a 360° circular orbit with 64 stops for 30-sec acquisition (step-and-shoot technique).

The ^{99m}Tc(V)-DMSA planar and SPECT images were compared with chest radiographs and XCT. Accumulation in lung tumors was evaluated on SPECT images visually and by the uptake index and correlated with tumor histology. Tumor sizes were obtained either from pathological specimen (P) or CT imaging measurement (C). Visual interpretation was done consenually by three radiologists, and accumulation of radiotracer was visually divided into four degrees: 0, uptake similar to the surrounding normal lung parenchymal tissue; I, uptake above the normal lung tissue; II, uptake between I and III; and III, uptake similar to or above the blood-pool activity in the major cardiovascular structures. Regions of interest (ROIs) were drawn over the lesion (L) and contralateral normal lung tissue (N), and maximum and average counts were obtained.

Since a malignant tumor may often involve different tissues such as highly malignant tissue, normal residual tissue, necrotic tissue, etc., and the most aggressive part of a tumor might be represented by the area of the maximum counts, we decided to normalize the maximum counts in the tumor to the average counts in the normal region. Maximum counts in the normal contralateral region may not reflect true homologous tissue, therefore, we calculated uptake ratio (L/N ratio) based on maximum counts in the tumor normalized to average counts in the homologous region.

Since we expected some difference in ^{99m}Tc(V)-DMSA uptake

TABLE 1
Clinical Findings

Patient no.	Age (yr)	Sex	Cell type	Tumor staging	Tumor size (cm)	Metastasis (N/B)	Uptake (PT/B)	Grading	L/N ratio
1	36	M	AdenoCa	p-$T_1N_0M_0$ (St.I)	2.2 × 2.0 × 2.0 (P)	N(−)/B(−)	PT(+)/B(−)	III	3.11
2	61	M	AdenoCa	p-$T_3N_2M_0$ (St.IIIA)	7.0 × 4.0 × 7.5 (P)	N(+)/B(−)	PT(+)/B(−)	III	3.04
3	67	F	AdenoCa	p-$T_2N_0M_0$ (St.I)	3.5 × 3.5 × 3.6 (P)	N(−)/B(−)	PT(+)/B(−)	III	1.78
4	71	F	AdenoCa	p-$T_2N_1M_1$ (St.IV)	3.8 × 2.5 × 3.3 (P)	N(+)/B(−)	PT(+)/B(−)	III	2.08
5	75	M	AdenoCa	p-$T_2N_0M_0$ (St.I)	4.5 × 3.6 × 3.3 (P)	N(−)/B(−)	PT(+)/B(−)	III	1.91
6	62	F	AdenoCa	c-$T_1N_0M_1$ (St.IV)	2.3 × 2.1 × 2.1 (C)	N(−)/B(+)	PT(+)/B(+)	II	2.14
7	72	F	AdenoCa	p-$T_2N_2M_1$ (St.III)	3.7 × 3.0 × 2.5 (P)	N(+)/B(−)	PT(+)/B(−)	II	2.01
8	73	M	AdenoCa	p-$T_2N_0M_1$ (St.IV)	3.6 × 4.0 × 4.5 (P)	N(−)/B(−)	PT(+)/B(−)	II	1.72
9	54	F	AdenoCa	p-$T_1N_0M_0$ (St.I)	2.3 × 2.1 × 1.8 (P)	N(−)/B(−)	PT(+)/B(−)	I	1.51
10	68	M	AdenoCa	p-T_2N_0Mx (St.I)	6.0 × 4.8 × 2.5 (P)	N(−)/B(x)	PT(+)/B(−)	I	1.36
11	66	F	AdenoCa	p-$T_1N_0M_0$ (St.I)	2.5 × 2.3 × 2.0 (P)	N(−)/B(−)	PT(+)/B(−)	I	1.28
12	58	F	AdenoCa	p-$T_1N_0M_1$ (St.IV)	1.8 × 1.3 × 1.2 (P)	N(−)/B(+)	PT(−)/B(+)	0	—
13	83	F	AdenoCa	p-$T_2N_0M_0$ (St.I)	3.5 × 3.1 × 2.5 (P)	N(−)/B(−)	PT(−)/B(−)	0	—
14	64	M	AdenoCa	p-$T_1N_3M_1$ (St.IV)	2.0 × 2.5 × 2.5 (P)	N(+)/B(+)	PT(−)/B(+)	0	—
15	72	M	SCC	p-$T_2N_1M_0$ (St.II)	6.0 × 7.0 × 7.5 (P)	N(+)/B(−)	PT(+)/B(−)	III	2.94
16	80	M	SCC	c-$T_2N_1M_0$ (St.II)	2.0 × 3.0 × 2.5 (C)	N(+)/B(−)	PT(+)/B(−)	III	2.71
17	69	M	SCC	c-$T_1N_0M_0$ (St.I)	5.5 × 4.5 × 4.0 (C)	N(−)/B(−)	PT(+)/B(−)	III	2.82
18	71	M	SCC	p-T_3N_0Mx (St.IIIA)	4.3 × 4.8 × 6.0 (P)	N(−)/B(x)	PT(+)/B(−)	III	2.52
19	62	M	SCC	p-T_2N_2Mx (St.IIIA)	2.3 × 3.4 × 5.0 (P)	N(+)/B(x)	PT(+)/B(−)	III	2.37
20	67	M	SCC	p-$T_2N_0M_0$ (St.II)	7.5 × 4.5 × 8.0 (P)	N(−)/B(−)	PT(+)/B(−)	III	2.30
21	70	M	SCC	p-$T_2N_1M_0$ (St.IIIB)	3.4 × 3.6 × 5.0 (P)	N(+)/B(−)	PT(+)/B(−)	III	2.18
22	69	M	SCC	p-$T_3N_2M_0$ (St.IIIA)	3.5 × 3.5 × 4.0 (P)	N(+)/B(−)	PT(+)/B(−)	III	2.02
23	61	F	SCC	c-$T_2N_2M_1$ (St.IV)	8.5 × 7.5 × 12 (C)	N(+)/B(−)	PT(+)/B(−)	III	1.91
24	62	M	SCC	c-T_4N_2Mx (St.III)	3.0 × 2.3 × 2.5 (C)	N(+)/B(x)	PT(+)/B(−)	II	1.83
25	78	M	SCC	p-T_2N_0Mx (St.I)	2.5 × 2.2 × 4.0 (P)	N(−)/B(x)	PT(+)/B(−)	I	1.62
26	65	M	Large CC	p-$T_3N_1M_0$ (St.IIIA)	6.0 × 6.5 × 7.0 (P)	N(+)/B(−)	PT(+)/B(−)	III	2.70
27	48	M	Small CC	c-$T_3N_3M_0$ (St.IIIB)	5.0 × 4.5 × 6.0 (C)	N(+)/B(−)	PT(+)/B(−)	III	2.83
28	75	M	Carcinoid	c-$T_2N_1M_1$ (St.IV)	4.0 × 3.5 × 2.5 (C)	N(+)/B(+)	PT(+)/B(+)	III	2.34
29	66	F	Benign	*	2.0 × 3.0 × 4.0 (C)	N(−)/B(−)	PT(−)/B(−)	0	—
30	75	F	Benign	*	2.0 × 2.0 × 2.5 (C)	N(−)/B(−)	PT(−)/B(−)	0	—
31	23	F	Benign	*	2.0 × 2.0 × 2.0 (C)	N(−)/B(−)	PT(−)/B(−)	0	—

*No histological evidence but no change for more than 2 yr of follow-up.

(P) and (C) represent pathological specimen measurements and CT scanning measurements respectively. Metastasis (N = mediastinal node involvement/B = bone metastasis) was investigated with pathological specimen (P), CT and bone scintigraphy. PT = primary tumor; L/N ratio is the maximum lesion counts/mean normal lung tissue counts.

in malignant tumors, we compared uptake ratio versus tumor histology with correlation coefficient. Tumor volume was roughly calculated by multiplying three-dimensional measurements. We compared tumor volume versus uptake ratio with one-sided unpaired Student's t-test.

RESULTS

Table 1 presents the clinical findings and ^{99m}Tc(V)-DMSA uptake for all patients examined. Thirty-one patients with a lung tumor had 28 primary lung cancers with four osseous metastatic foci and three benign lesions; 14 adenocarcinomas with 3 osseous metastases, 11 SCC, one large-cell carcinoma, one small-cell carcinoma, one bronchial carcinoid tumor with bone metastasis. Three lesions were considered to be benign by interval resolution and/or no interval change by intense follow-up examinations over 2 yr and were negative on ^{99m}Tc(V)-DMSA SPECT images. There were three false-negative lesions of 14 adenocarcinomas. No false-positives for the primary lung cancer were seen in this small study. There was an area of increased uptake noted in the right atrium in two patients, and an area of intense uptake in the sterno-clavicular joint and sterno-manubrial joint in two patients. There was no

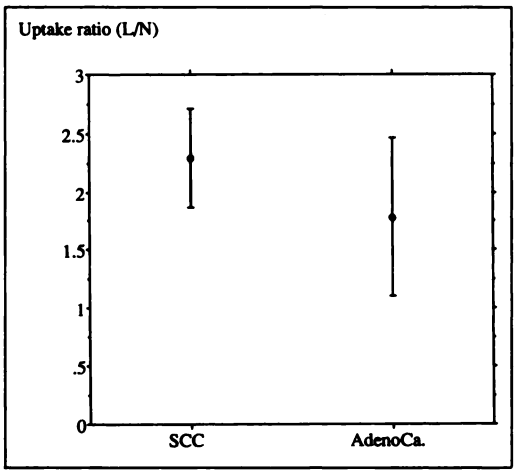

FIGURE 1. Uptake ratio between SCC and adenocarcinoma.

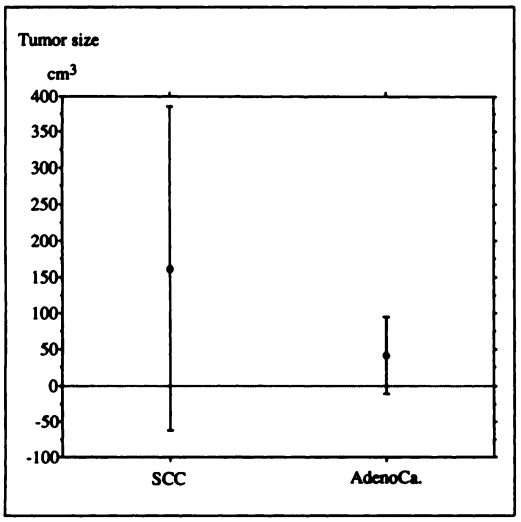

FIGURE 2. Tumor size.

increased uptake in the thyroid glands but matured breast tissue normally accumulated ^{99m}Tc(V)-DMSA. Tumor extension into the mediastinum or nodal involvement of the mediastinum was difficult to evaluate by persistent blood-pool activity in the major cardiovascular structures, therefore, 14 cases with mediastinal node involvement were not evaluated. The uptake ratio of 14 adenocarcinomas was 1.78 ± 0.68 (mean ± s.d.) and 11 SCCs showed an uptake ratio of 2.29 ± 0.43 (mean ± s.d.). A large-cell carcinoma was 2.70, a small-cell carcinoma was 2.83 and a bronchial carcinoid tumor was 2.34. The uptake ratio of the squamous cell carcinomas (2.29 ± 0.43) was higher than that of the adenocarcinomas (1.78 ± 0.68) ($p < 0.05$) (Fig. 1). The calculated average tumor volume of SCC (161.5 ± 224.5 cm^3) was larger than that of adenocarcinomas (41.7 ± 53.3 cm^3) (mean ± s.d.) ($p < 0.07$) (Fig. 2). But there was no significant correlation between tumor size and uptake ratio in either adenocarcinoma or SCC.

Patient One

A 36-yr-old male was admitted for evaluation of an abnormal shadow on a chest radiograph taken during a routine medical examination. A 2 × 2 cm coin lesion was noted in the right mid-lung field (Fig. 3A).

Technetium-99m(V)-DMSA planar and SPECT images demonstrated an abnormal accumulation corresponding to the pulmonary lesion (Fig. 3B, C). The uptake ratio was 3.11. Surgical findings proved a 2.2 × 2.0 × 2.0 cm poorly differentiated adenocarcinoma in S3 of the right upper lobe of pathological stage $T_1N_0M_0$ (Stage I).

Patient Two

A 62-yr-old female complained of gait disturbance and left hemiparesis. A chest radiograph showed abnormal shadow in the left pulmonary hilum and brain CT also showed cerebral metastatic lesions. Pentavalent ^{99m}Tc-DMSA planar image demonstrated mildly increased uptake in the lung tumor and an area of intense uptake in the right humerus (Fig. 4). The uptake ratio was 2.14. Cytological examination proved adenocarcinoma and the clinical stage was $T_1N_0M_1$ (Stage IV).

Patient Three

A 72-yr-old male had a large abnormal shadow in the right lower lung (Fig. 5A). Pentavalent ^{99m}Tc-DMSA planar and SPECT images showed a ring-like area of increased uptake corresponding to the pulmonary lesion (Fig. 5B, C). The uptake ratio was 2.94. Surgical findings proved a 6.0 × 7.0 × 7.5 cm SCC in the right lower lobe invading into the right middle lobe with a large area of central necrosis; the pathological stage was $T_2N_1M_0$ (Stage II).

Patient Four

A 65-yr-old male complained of left shoulder pain. A chest radiograph demonstrated a large mass in the left apex (Fig. 6A). Chest CT showed a left apical mass with chest wall invasion (Fig. 6B). Technetium-99m(V)-DMSA planar image demonstrated increased uptake in the left apex (Fig. 6C) and SPECT images showed an oval-shaped area of increased uptake with a central defect corresponding to the pulmonary lesion (Fig. 6D). The uptake ratio was 2.70. Surgical findings proved a 6.0 × 6.5 × 7.0 cm large-cell carcinoma in the left upper lobe (S_2) with chest wall invasion; the pathological stage was $T_3N_1M_0$ (Stage IIIA).

FIGURE 3. Chest radiograph (A) shows a coin lesion in the right mid-lung field laterally (arrowhead). Technetium-99m(V)-DMSA planar image (B) showed increased uptake corresponding to the lesion (arrowhead). Technetium-99m(V)-DMSA coronal SPECT image (C) demonstrates an area of intense uptake in the lung lesion (arrow).

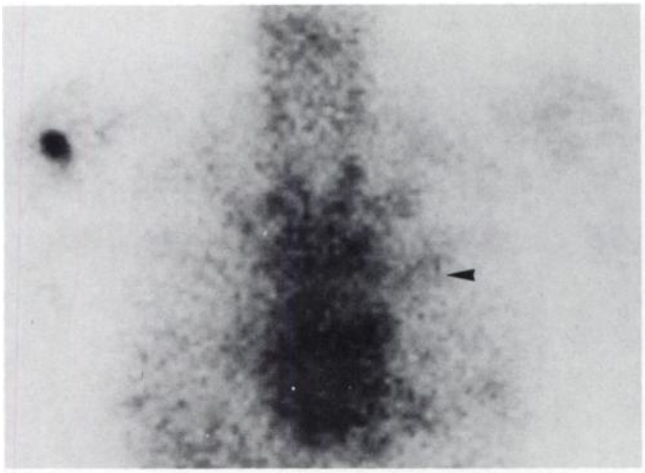

FIGURE 4. Technetium-99m(V)-DMSA planar image shows an area of mildly increased uptake in the left pulmonary hilum (arrow) and an area of intense uptake in the right proximal humerus corresponding to the osseous metastatic lesion.

Patient Five

A 75-yr-old male complained of back pain with right inguinal mass. A chest radiograph demonstrated abnormal shadow in the left pulmonary hilum (Fig. 7A). Chest CT showed a 4.0 × 3.5 × 2.5 cm mass in the left hilum adjacent to the left pulmonary artery and a metastatic lesion to the thoracic vertebral body (Fig. 7B). Pentavalent technetium-99m-DMSA planar and SPECT images showed an area of increased uptake corresponding to the left pulmonary hilar lesions (Figs. 7C and D) and a metastatic lesion in the thoracic spine (Fig. 7E). Uptake ratio was 2.34. Lung biopsy revealed carcinoid tumor of the lung and clinical stage was $T_2N_1M_1$ (Stage IV).

DISCUSSION

Our results demonstrate that 89% of the primary lung cancers were visualized by ^{99m}Tc(V)-DMSA SPECT imaging and the average uptake ratio was higher in SCCs (2.29 ± 0.43) than adenocarcinomas (1.78 ± 0.68) ($p < 0.05$). Uptake ratio was calculated by maximum counts in the tumor normalized to average counts in the homologous normal lung region. We expected that the most aggressive part of a tumor might be represented by the area of maximum counts. Benign pulmonary lesions did not accumulate ^{99m}Tc(V)-DMSA. There was some discrepancy between visual grading and uptake ratio in the lesions near the cardiovascular structures, visual grading scores tended to decrease in such lesions because of persistent blood-pool activity. Mediastinal tumor extension and small nodal lesions could not be detected or differentiated from the vascular structures. Fourteen patients with positive mediastinal involvement on CT or surgical investigation could not be evaluated in this study.

Watkins et al. reported that there was no evidence of active uptake of ^{99m}Tc(V)-DMSA by SCC, and the tumors appeared to exhibit a prolonged washout phase of radioactivity when compared to the blood pool (*12*). From our experience ^{99m}Tc(V)-DMSA has been observed to accumulate in the active healing scar tissue, early phase of healing bony reaction and young breast tissue, where there seems to be increased protein metabolism for fibrous tissue, osteoid and proliferative glandular tissue formation. The mechanism of tumor accumulation of the ^{99m}Tc(V)-DMSA has not been well understood but we believe that ^{99m}Tc(V)-DMSA is taken up by the tumor cells, as it shows a similarity to phosphate molecules which accumulate due to increased protein metabolism.

With reference to histologic type in lung cancers, Togawa et al. (*14*) reported that adenocarcinoma showed a higher accumulation of ^{201}Tl-Cl than SCC. The mechanism of tumor accumulation of these two compounds would be different, and ^{201}Tl-Cl tumor uptake is believed to depend upon the active transport mechanism and blood perfusion. Once ^{201}Tl-Cl accumulates in a tumor tissue, its characteristic behavior used to differentiate between a benign and malignant tumor is mainly dependent upon the difference in washout phase, which may reflect disturbed membrane transport mechanism caused by tumor change.

FIGURE 5. Chest radiograph (A) shows a large mass in the right lower lung field medially. Technetium-99m(V)-DMSA planar image (B) shows a curvilinear area of increased uptake in the right lower lung (arrowheads). Technetium-99m(V)-DMSA axial SPECT image (C) demonstrates a ring-like area of increased uptake corresponding to the lesion of peripheral viable tumor (arrows) with a large central necrosis.

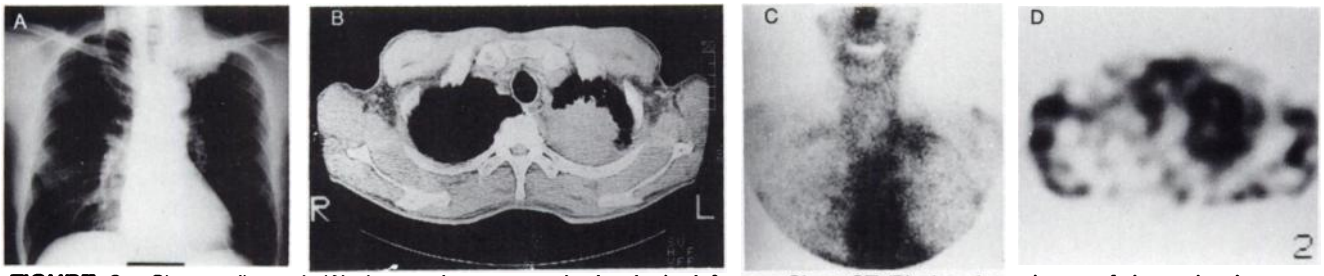

FIGURE 6. Chest radiograph (A) shows a large mass shadow in the left apex. Chest CT (B) also shows large soft tissue density mass in the left apex. Pentavalent technetium-99m-DMSA planar image (C) demonstrated an area of increased uptake in the left apex (arrow). Pentavalent technetium-99m-DMSA axial SPECT image (D) reveals oval-shaped, rim-like uptake corresponding to the tumor.

It is interesting that there seems to be a difference in ^{99m}Tc(V)-DMSA accumulation among histologic tumor types, higher uptake ratio in the SCC than the adenocarcinoma, and no uptake in the benign pulmonary lesions. The calculated average tumor volume was evidently larger in SCC (161.5 ± 224.5 cm^3) than in adenocarcinomas (41.7 ± 53.3 cm^3) (mean ± s.d.) ($p < 0.07$); however, there was no statistically significant correlation between tumor size and uptake ratio in either adenocarcinoma or SCC. This could not explain that a larger tumor can always show higher uptake of ^{99m}Tc(V)-DMSA. We thought that there was something different from the tumor size to explain different uptake ratio.

Osseous metastatic lesions were clearly visualized by ^{99m}Tc(V)-DMSA planar and SPECT images. The uptake was well localized and intense in comparison with the rest of the normal osseous structures. Although the mechanism of tumor uptake has not been clear, the osseous metastatic lesions (Table 1, Patients 12 and 14), whose primary lesions did not accumulate ^{99m}Tc(V)-DMSA, demonstrated intense uptake. Something different seemed to happen in the metastatic lesions, such as increased blood perfusion or reactive bony change causing increased osteoid formation. Pentavalent ^{99m}Tc-DMSA also demonstrated increased uptake in a case of benign lesion in the sterno-clavicular and the sterno-manubrial joint, but it was not difficult to differentiate the benign lesion from metastatic malignant lesions because of their locations. There were two cases showing an area of increased uptake in the right atrium, although the reason of this uptake was not known.

Pentavalent technetium-99m-DMSA SPECT study seems to be an useful noninvasive method to detect malignant pulmonary lesions and osseous metastatic foci as well as to differentiate malignant lesions from benign conditions. The mechanism of tumor accumulation of ^{99m}Tc(V)-DMSA is not clear, but ^{99m}Tc(V)-DMSA could be taken up by the tumor cells in a similar mechanism to phosphate molecules which are accumulated due to increased protein metabolism. Three cases (Table 1: Patients 15, 20 and 26) in our study showed a necrotic center in the tumor on pathologic specimen and ^{99m}Tc(V)-DMSA demonstrated a central defect and a peripheral ring-like accumulation corresponding to the necrotic center and peripheral viable tumor tissue respectively (Figs. 5 and 6). This could raise the possibility to detect viable or residual tumor after radiation or chemotherapy depending upon the increased protein metabolism by the tumor cells, especially in the osseous metastatic lesions.

REFERENCES

1. Westera G, Gadze A, Horst W. A convenient method for the preparation of ^{99m}Tc(V) dimer-captosuccinic acid (^{99m}Tc(V-DMSA). *Int J Appl Radiat Isot* 1985;36:311–312.
2. Blower PJ, Singh J, Clarke SEM. The chemical identity of pentavalent technetium-99m-dimercaptosuccinic acid. *J Nucl Med* 1991;32:845–849.

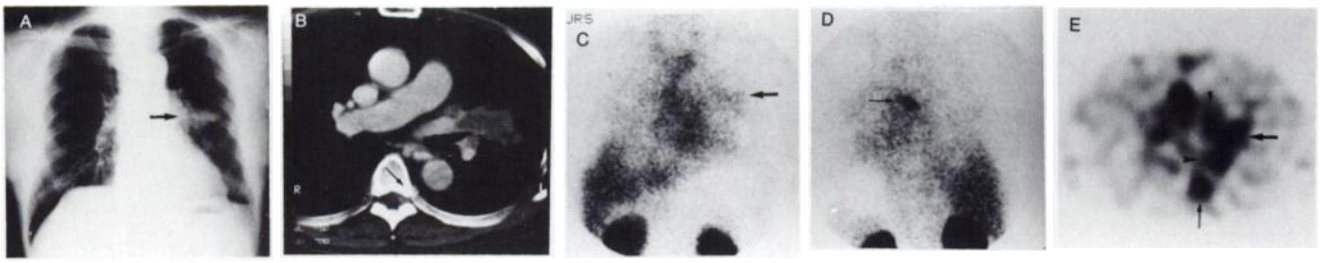

FIGURE 7. Chest radiograph (A) shows a mass shadow in the mid-lung field extending from the left pulmonary hilum (arrow). Chest CT (B) shows a mass density lateral to the left pulmonary artery and metastatic lesion in the thoracic spine (small arrow) postero-medial to the descending aorta. Pentavalent technetium-99m-DMSA anterior planar image (C) demonstrates an area of increased uptake in the left mid-lung field (arrow) and posterior planar image (D) demonstrates an area of intense uptake in the mid-thoracic spine (small arrow). Pentavalent technetium-99m-DMSA axial SPECT image (E) demonstrates an area of increased uptake (arrow) lateral to the left pulmonary artery (small arrowhead) and anterior to the descending aorta (arrowhead), and an area of intense uptake (small arrowhead) corresponding to the metastatic lesion of the thoracic spine.

3. Abrams MJ. Small coordination complexes in tumor imaging [Editorial]. *J Nucl Med* 1991;32:849–850.
4. Ohta H, Yamamoto K, Endo K, et al. A new imaging agent for medullary carcinoma of the thyroid. *J Nucl Med* 1984;25:323–325.
5. Clarke SEM, Lazarus CR, Wraight P, et al. Pentavalent (^{99m}Tc)DMSA, (I-131)MIBG, and (^{99m}Tc)MDP: an evaluation of three imaging techniques in patients with medullary carcinoma of the thyroid. *J Nucl Med* 1988;29: 33–38.
6. Lette J, Monier D, Ledoux R, et al. False-positive Tc-99m pentavalent DMSA uptake in the imaging of medullary carcinoma of the thyroid. *Clin Nucl Med* 1991;16:136–137.
7. Ohta H, Endo K, Fujita T, et al. Imaging of head and neck tumors with technetium(V)-99m DMSA, a new tumor-seeking agent. *Clin Nucl Med* 1985;10:855–860.
8. Ohta H, Endo K, Fujita T, et al. Clinical evaluation of tumor imaging using ^{99m}Tc(V) dimercaptosuccinic acid, a new tumor-seeking agent. *Nucl Med Commun* 1988;9:105–116.
9. Lamki L, Shearer R. Tc-99m-DMSA uptake by metastatic carcinoma of the prostate. *J Nucl Med* 1985;25:733–734.
10. Watkins JC, Lazarus CR, Mistry R, et al. Technetium-99m(V)dimercaptosuccinic acid uptake in patients with squamous carcinoma of the head and neck-experience in imaging. *J Nucl Med* 1989;30:174–180.
11. Watkins JC, Allen S, Lazarus CR, et al. What is the optimal imaging time for ^{99m}Tc(V)DMSA planar scintigraphy in the detection of squamous carcinoma? A comparative study in humans and in an animal tumor model. *Nucl Med Commun* 1989;10:741–750.
12. Watkins JC, Allen SJ, Laws DE, et al. The pharmacokinetics and biodistribution of technetium-99m(V)dimercaptosuccinic acid in an animal tumor model. *J Nucl Med* 1991;32:1235–1238.
13. Hirano T, Tomiyoshi K, Ying Jian Zhang, et al. Preparation and clinical evaluation of ^{99m}Tc-DMSA for tumor scintigraphy. *Eur J Nucl Med* 1994; 21;82–85.
14. Togawa T, Suzuki A, Higuchi Y, et al. Thallium-201 to ^{67}Ga crude uptake ratio in primary lung cancer with reference to histological type. *Lung Cancer* 1985;25:187–195.

EDITORIAL

Tissue Characterization in Nuclear Oncology: Its Time Has Come

In this issue of the *Journal*, Hirano et al. proposed methodology for producing ^{99m}Tc(V)-DMSA from a kit (*1*) presents a new role for nuclear medicine imaging in oncology: characterization of lung cancer. Various types of lung cancers were visualized with ^{99m}Tc(V)-DMSA (90%) in their study, but the semiquantitative target-to-background ratio was higher in squamous-cell carcinoma than in the adenocarcinoma or metastatic bone lesions. Moreover, benign lesions did not take up ^{99m}Tc(V)-DMSA.

Technetium-99m-(V)-DMSA is only one of several imaging agents that are undergoing clinical or experimental trials in producing images that can reflect the character of the tissues. Several other radiopharmaceuticals currently used or that are potentially useful in discriminating tumor masses and characterizing malignant tissues include: (1) radioelement pharmaceuticals such as ^{67}Ga and ^{201}Tl; (2) tumor characterizing organic compounds such as ^{99m}Tc-sestamibi for SPECT, ^{18}F-fluorodeoxyglucose (FDG) for PET; and (3) peptides and cutting edge radiopharmaceuticals such as receptor imaging peptides, single-chain binding proteins and biologically active peptides, as well as several experimental tumor imaging agents.

Received Oct. 24, 1994; accepted Oct. 24, 1994.
For correspondence or reprints contact: Lamk M. Lamki, MD, University of Texas Health Science Center, Department of Radiology, 6431 Fannin, MSB 2.132, Houston, Texas 77030.

Radioelement Pharmaceuticals

Gallium-67, ^{201}Tl SPECT and planar imaging emerged in the 1980s as major functional imaging tools in oncology. They are both radioisotopes of naturally occurring elements and are commercially available as ^{67}Ga-citrate and ^{201}Tl-chloride. Although ^{67}Ga imaging has been used for years as a tumor marker in nuclear imaging, recent efforts have begun to assess its potential role in tissue characterization to differentiate recurrent tumors from necrotic mass after radiotherapy or chemotherapy. Masses identified on a follow-up CT scan as lymphoma and other tumors have been successfully differentiated by ^{67}Ga (*2,3*). The high uptake of this nonspecific radiopharmaceutical indicates the viability of tumor malignancy. Gallium-67 is used to detect not only effectiveness of therapy in oncology, but also prognostication of outcome (*4,5*). The shift toward tissue characterization and higher specificity in nuclear oncology is highlighted by the increasing use of ^{201}Tl instead of ^{67}Ga in tumor characterization.

Thallium-201 imaging in the follow-up of post-therapy brain tumors has been found to be most helpful in discriminating residual postradiation necrotic tissue from recurrent or residual viable tumor (*6–8*). A major attraction of ^{201}Tl imaging over ^{67}Ga is the time needed to complete the study: 3–4 hr versus 48–72 hr needed for imaging with ^{67}Ga. Thallium-201 is also more specific than ^{67}Ga in a variety of brain, breast and mediastinal tumors (*7–10*). When used conjointly with ^{67}Ga, however, ^{201}Tl can identify Kaposi's sarcoma and differentiate it from lymphoma in HIV-positive patients (*9,10*). The retention index of ^{201}Tl, which compares the early target-to-background ratio with the delayed ratio (1 to 3 hr later), has been found to be highly accurate in identifying tumor viability after chemotherapy and radiotherapy (*11–13*). Suga et al. (*14*) used ^{201}Tl in experimental monitoring of radiotherapeutic effects of tumor proliferative potential after treatment. Other clinicians also have found thallium's retention index to be useful in characterizing histological types of tumors (*6,15*). Thallium-201 imaging also has been used in breast cancer (*16,17*) to separate benign from malignant lesions prior to biopsy in patients who had an equivocal or inconclusive mammogram [but has been found to have a slightly lower negative predictive value than sestamibi (96%